Electrochemical Control of Strong Coupling of CdSe Exciton-Polaritons in Plasmonic Cavities

Nathan G. Sinai*¹, Christian Y. Dones Lassalle*², Jennica E. Kelm*², Shreya K. Patel¹, Sang-Min Park¹, Max J.H. Tan¹, Teri W. Odom^{1,1} and Jillian L. Dempsey^{1,2}

*These authors contributed equally to this work.

†Co-corresponding authors

¹Department of Chemistry, Northwestern University, Evanston, IL 60208

²Department of Chemistry, University of North Carolina, Chapel Hill, North Carolina 27599-3290,

United States

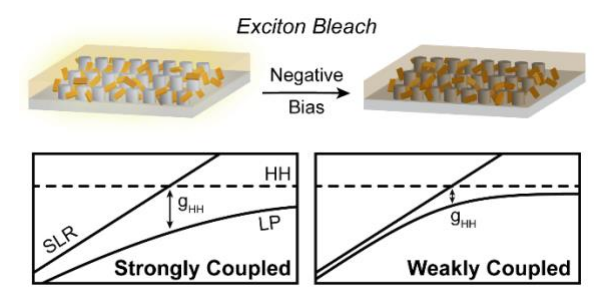
Abstract (129/150 words)

This work reports *in-situ* (active) electrochemical control over the coupling strength between semiconducting nanoplatelets and a plasmonic cavity. We found that by applying a reductive bias to an Al nanoparticle lattice working electrode, the number of CdSe nanoplatelet emitters that can couple to the cavity is decreased. Strong coupling can be reversibly recovered by discharging the lattice at oxidative potentials relative to the conduction band edge reduction potential of the emitters. By correlating the number of electrons added or removed with the measured coupling strength, we identified that loss and recovery of strong coupling is likely

hindered by side processes that trap and/or inhibit electrons from populating the nanoplatelet conduction band. These findings demonstrate tunable, external control of strong coupling and offer prospects to tune selectivity in chemical reactions.

<u>Keywords:</u> Exciton-polariton, CdSe nanoplatelets, nanoparticle lattice cavity, electrochemical control

<u>TOC</u>



Exciton-polaritons are hybrid light-matter quasiparticles that form under strong coupling, which occurs when the coupling between an optical cavity and an exciton exceeds the losses of either. 1-2 Exciton-polaritons are important in diverse fields, ranging from quantum computing 3 to sensing 4 to low-threshold lasing. 5 Recently, these quasiparticles have gained attention to control the product distribution of chemical reactions by altering potential energy surfaces. 6 However, most work on polariton-mediated charge transfer, 7 singlet fission, 8 and reaction control 9 has been limited to theory; there are few experiments that have demonstrated exciton-polariton-mediated chemical reactivity. 10-11

One key parameter to control reactivity is the coupling strength (g) between many (N) emitters and a cavity:¹²

$$g = \sqrt{N} \cdot \mu \sqrt{\frac{\hbar \omega}{2\epsilon_0 V_c}}$$

where μ is the transition dipole moment of the emitter, ω is the frequency of a photon resonant to the cavity, and V_c is the mode volume of the cavity. Active tuning (i.e., external, *in-situ* control)¹³⁻¹⁴ of g often requires complex means, including varying the refractive index environment through microfluidics¹⁵ or raising the temperature of the emitters.¹⁶ Ideally, manipulating g should occur in a simple, non-invasive manner, such that polariton-mediated reactions can be studied without compounding effects. Adjusting the coupling strength by segregating emitters from the cavity is one proposed approach to influence the product distribution of chemical reactions resulting from polariton-altered frontier molecular orbitals of reagents.¹⁷

Populating or depleting frontier molecular orbitals by applying an electrochemical potential is known to change the optical properties of molecular species and therefore exciton formation.¹⁸ Similarly, when a negative (positive) potential of appropriate magnitude is applied to semiconducting excitonic materials, electrons (holes) are injected into the conduction (valence) band of the emitters. With the conduction band occupied (or valence band depleted), electronic

transitions cannot occur, and optical absorptions are bleached. As a result, in an ensemble of *N* semiconductor excitons under reductive bias, fewer emitters are available to couple to the cavity. Although electrical¹⁹⁻²⁰ and electrochemical²¹⁻²³ tunability of coupling strength has been realized, the focus has been on either organic dyes or transition metal dichalcogenide (TMD) flake emitters. CdSe nanoplatelets (NPLs) have advantages because of their large oscillator strengths²⁴⁻²⁶ compared to organic emitters and their ease of ligand exchange compared to TMDs²⁷⁻³⁰ and are established materials for strong coupling to a variety of cavities at room temperature.³¹⁻³² Since CdSe NPLs can be synthesized with a variety of absorption and emission energies based on plate thickness,³³ they can be used to target a broad range of reaction energetics.

Plasmonic nanoparticle lattices are advantageous cavities for strong coupling and for carrying out chemical reactions due to their open lattice structure.³⁴⁻³⁷ Periodic lattices of metallic nanoparticles can support high-quality surface lattice resonance (SLR) cavity modes by coupling the localized surface plasmons of each nanoparticle to the diffractive photonic modes in the lattice in an index-matched environment.³⁸⁻³⁹ The single substrate and metal nanoparticles of the cavity facilitate incorporation into spectroelectrochemistry experiments, as the cavity is accessible to solvents and reagents, and the lattices can be fabricated on transparent conductive substrates.³⁷ By tuning nanoparticle material and shape as well as periodicity, plasmonic lattice cavities can be designed to interact with different excitonic materials.³⁹

Here we show external, *in-situ* control of the coupling strength in polaritons formed between CdSe NPL excitons and a plasmonic lattice cavity. Polariton coupling strength was modulated via an applied electrochemical potential to an Al nanoparticle lattice on an indium tin oxide substrate that functioned as the working electrode. By applying reductive potentials, we incrementally raised the Fermi level of a subset of CdSe NPLs in the film. When the magnitude of that potential exceeded the formal reduction potential of the conduction band edge, the excitonic absorption features of the NPLs bleached. Repeated cycles beyond the conduction

band edge were found to suppress the coupling strength between the cavity and NPLs. Under oxidative applied potentials, the NPL film discharged, and the polariton features were recovered. The extent of the reduction and recovery in coupling strength correlated directly with the number of electrons added or removed from the NPL film, a connection yet to be formalized in the literature. External, *in-situ* control of the degree of coupling will enable future experiments that take advantage of polariton-mediated reactions.

We designed a custom-built, three-electrode cell for spectroelectrochemical experiments on the coupled lattice cavity–NPL film system (**Figure 1a**). The transparent working electrode functions as one window, and a second inert window confines the electrolyte solution. The Ag/AgNO₃ reference electrode and Pt wire counter electrode complete the cell and were mounted offset so as not to obstruct the transmission of light through the cell under an applied potential. This architecture allows the electrochemical cell to be mounted into a Fourier transform microscope between a condenser and objective lens^{5, 40} so that changes to polaritons as a result of bias can be quantified in real time (**Figure 1b**).

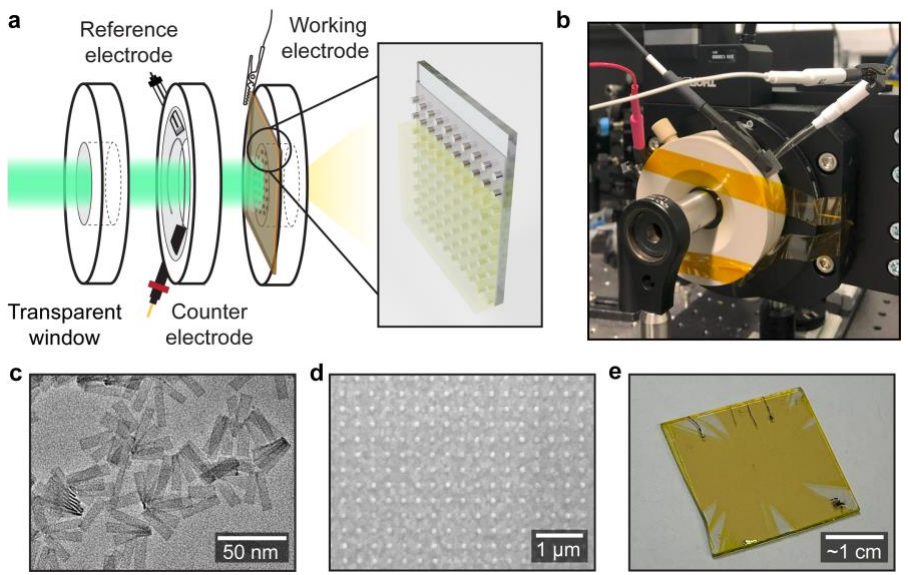
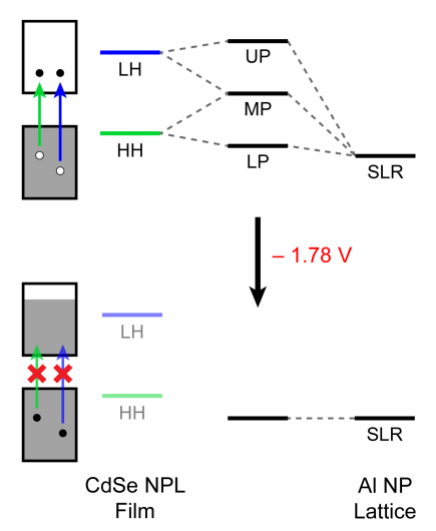


Figure 1: Spectroelectrochemical cell for active tuning of exciton polaritons. (a)

Diagram of the cell showing the sandwiched cell design with space for an electrolyte solution, reference, and counter electrodes. (inset) Detailed model NPL film in the dual-function aluminum nanoparticle cavity on the working electrode ITO glass substrate (b) Photograph of the cell showing integration with the Fourier transmission microscope. (c) TEM image of monodisperse ~ 10 nm x 30 nm CdSe NPLs used in film. (d) SEM image of $a_0 = 320$ nm periodicity lattice fabricated on ITO. (e) Optical micrograph of 2.5 x 2.5 cm ITO-glass substrate patterned with 300 μ m x 300 μ m Al nanoparticle lattice and CdSe NPL film.

Four-monolayer, oleate-capped CdSe NPLs (**Figure 1c**) were synthesized using our improved procedure⁵ and cast into an 110-nm thick film. There are two excitonic transitions in CdSe NPLs: (1) the heavy hole (HH) valence band to the conduction band at 2.41 eV (~514 nm) and (2) the light hole (LH) valence band to the conduction band at 2.58 eV (~480 nm).³³ Photonic cavities consisting of square lattices of Al nanoparticles (diameter d = 90 nm, height h = 60 nm) with periodicity $a_0 = 320$ nm (**Figure 1d**) were fabricated by electron beam lithography on ITO-coated

glass slides (Supporting Information). The emitter-cavity system consists of ITO on glass, an Al NP lattice, and a CdSe NPL film (**Figure 1e**). For electrochemical measurements, samples are immersed in 0.25 M [Bu₄N][PF₆] in CH₃CN electrolyte (Supporting Information) since CH₃CN is a polar solvent with low resistivity and stable in a wide potential window (~ 3 V to –3 V vs. SCE). If the SLR cavity mode is close enough in energy to the heavy or light hole (or both), polaritons can form. Typically, the higher energy eigenmode is referred to as the upper polariton (UP) while the lower energy mode is defined as the lower polariton (LP). Since CdSe NPLs support two excitonic absorptions, depending on the operational frequency of the cavity, a middle polariton (MP) mode can also be present. Scheme 1 summarizes how an applied bias can inhibit HH and LH excitonic transitions by populating the NPL conduction band with electrons. As a result, the HH and LH hole excitons are suppressed, which lowers the number of



Scheme 1: Fermi and energy level diagrams of the coupled CdSe NPL-Al lattice system with no voltage applied (top) and under a reductive potential (bottom).

available NPLs, N, that can couple to the cavity.

The conduction band edge potential of CdSe NPLs was quantified in UV-Vis absorbance spectroelectrochemical experiments of NPL films on Al lattice/ITO substrates (**Figure 2**). In these experiments, the applied potential was stepped from –0.94 to –2.34 V vs. Fc^{+/0}. The

potential range was selected to ensure that the transition from NPL emitters with unpopulated conduction bands to fully populated was resolved. 42-46 UV-vis absorbance spectra were collected with large reductive potential steps (100 mV) in the initial 400 mV of the range (from – 0.94 to –1.34 V vs. Fc^{+/0}) to minimize exposure of the sample to bias where no change in the absorbance profile was observed. Once bleaching of the LH and HH excitonic features occurred, spectra were collected every 50 mV (from –1.34 to –2.34 V) to track the bleach throughout the population of the conduction band and beyond (**Figure 2a**). After each reductive step, an oxidative step (–0.14 V vs. Fc^{+/0}) was applied to remove charges from the NPL film (i.e., the NPLs were discharged) and mitigate undesirable charging that may lead to degradation⁴⁷⁻⁴⁸ (Supporting Information). We did not observe electrochemical degradation of either the Al lattice or ITO film.

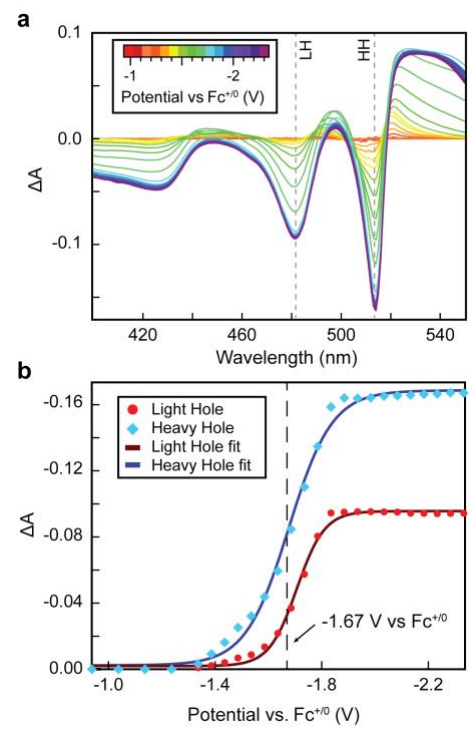


Figure 2: Quantified conduction band edge potentials. (a) Change in absorbance of CdSe NPL film on Al lattice cavity with an increasing applied potential showing the loss of absorbance from the HH and LH exciton transitions. (b) Fitting of the change in absorbance from the HH and LH exciton transitions vs. applied potential with a sigmoid curve to obtain the conduction band edge potential of −1.67 V vs. Fc^{+/0}. Each reductive and oxidative potential was applied for 35 s.

Figure 2a shows a progressive bleaching of the LH and HH absorption with increasing reductive potentials in the range of -1.40 to -1.85 V vs. Fc^{+/0}. Plots of the change in absorption (Δ A) of both the HH and LH transitions represent the fraction of reduced emitters as a function of applied potential (**Figure 2b**). These data can be fit to a sigmoidal function, as expected from the Nernst equation, and used to determine the formal reduction potential of the conduction band edge (-1.67 ± 0.06 V vs. Fc^{+/0}, see Supporting Information). Under such reductive bias, formation of the exciton is inhibited; we use this measured NPL conduction band edge potential as the starting bias to electrochemically tune the coupling in our system.

Figure 3a shows that the HH and LH excitonic transitions of CdSe NPL films are nondispersive, as expected. By varying the periodicity of the lattice, the Γ-point of SLR bands can be shifted higher or lower in energy.³⁸ We selected a_0 = 320 nm because this periodicity results in a distinct SLR mode whose Γ -point (k_{\parallel} = 0 μ m⁻¹, 2.26 eV) is lower in energy than the HH, and the most intense SLR bands crossing the HH relatively unobscured (Figure 3b). In order to perform the background correction and normalization required for spectroelectrochemical measurements, we only considered SLR modes excited under transverse electric (TE) polarization. The dispersion diagram of the bare Al nanoparticle lattice shows many modes because of the refractive index mismatch between the n = 1.525 superstrate and the ITO-glass substrate. Index oil was used for the uncoupled measurements to match the refractive index of glass to minimize the number of unique indices in the system. When the difference in refractive index is high, waveguide modes can form and couple to the SLR and generate waveguide-SLRs (W-SLR). 49-50 Based on finite-difference time-domain simulations (Supporting Information), we identify the lower energy dispersive X-shaped modes ($\Gamma = \sim 2.26 \text{ eV}$) as having predominantly dipolar character (SLR₁). The higher energy X-shaped mode ($\Gamma = \sim 2.56 \text{ eV}$) is also predominantly dipolar character (SLR₂), however the shift in energy is attributed to the SLR sensitivity to the local refractive index environment⁵¹⁻⁵² of either the ITO or the superstrate. The parabolic mode intersecting SLR₁ at k_{\parallel} = 0 μ m⁻¹ has increased field intensity in the ITO layer, and is likely a waveguide mode. For this electrochemical study of polaritons, we will only focus on the cavity mode described by SLR₁.

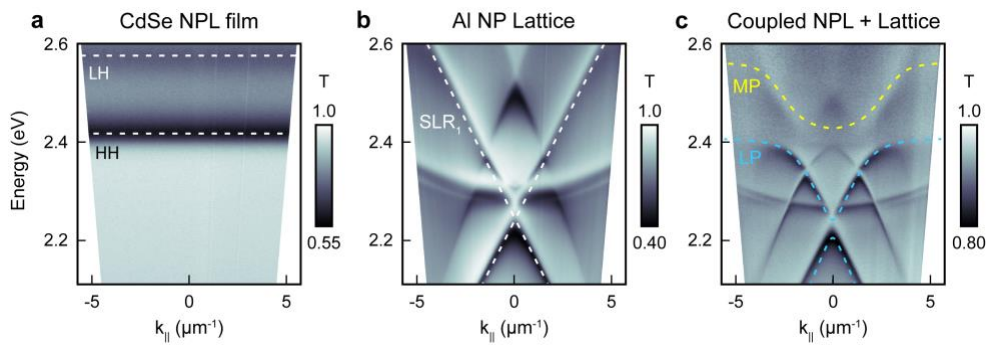


Figure 3: Strongly coupled CdSe NPL film to Al nanoparticle lattice cavity. (a)

Transmission from an uncoupled CdSe NPL film showing the non-dispersive light and heavy hole absorption bands. (b) TE-polarized transmission from an uncoupled a_0 = 320 nm Al lattice showing the dispersive SLR and waveguide modes, with the SLR of interest highlighted in yellow. (c) TE-polarized transmission from coupled CdSe NPL film and Al lattice cavity. Lower polaritons (green) and middle polariton (cyan) demonstrate anti-crossing behavior to deviate from the SLR dispersion at the HH energy.

Figure 3c depicts anti-crossing behavior characteristic of strong coupling between the SLR mode of the plasmonic cavity and the HH band of the NPL film at ca. k_{\parallel} = ±2.3 μm⁻¹ and 2.42 eV. The LP band occurs below the HH in energy and is overlaid with a teal dashed line based on a fit from the coupled oscillator model.^{5, 31} Below ~2.3 eV, the LP retains significant SLR character, matching the transmission from the uncoupled lattice. However, at energies close to the HH, the bands begin to bend outwards, resulting in flat bands at large k_{\parallel} reminiscent of the HH band. The MP, between the 2.42 and 2.58 eV, can likewise be fit and is traced in yellow. Similar to the LP, the MP has a more flat-band shape from the LH at larger k_{\parallel} values. However, the portion of the MP near the HH bends the opposite way, towards k_{\parallel} = 0 μm⁻¹. Fitting these features is more complicated because of the presence of both SLR₁ and SLR₂ modes. The UP would fall above the LH in energy out of the frame of the visualized area. By fitting the LP with the coupled oscillator model, we can extract a g_{HH} value that can be compared to the loss values (γ) of the HH exciton and SLR cavity (Supporting Information). The measurements

confirm that the coupling strength ($g_{HH} \approx 45 \text{ meV}$) is sufficiently large ($\gamma_{ex} = 40 \text{ meV}$, $\gamma_{ca} = 81 \text{ meV}$) to satisfy the criteria for strong coupling ($2g_{HH} > \gamma_{ex}$, γ_{ca}).

To tune the coupling strength as a function of applied potential, we performed a linear sweep voltammetry experiment, where the applied potential was swept from -1.53 V to -1.82 V vs. Fc^{+/0}. We observed a decrease in coupling at -1.74 V vs. Fc^{+/0} (Supporting Information). Informed by the reduction potential of the of the NPL conduction band edge (-1.67 V vs. Fc^{+/0}) and the change in coupling strength at -1.74 V vs. Fc^{+/0}, a step potential experiment was then performed by alternating between an applied reductive potential V_{app} of -1.78 V vs. Fc^{+/0} and a more positive discharging potential V_{dis} of -0.13 V vs. Fc^{+/0}, each for 35 s intervals. Significant charge injection into the NPL conduction band should occur at V_{app} , leading to a bleach of the excitonic absorption features and elimination of strong coupling. Charge can then be removed by applying the "discharge" step to restore strong coupling.

Figure 4 indicates that the coupling strength can be tuned from strong to the weak coupling under an applied voltage. Without V_{app} , the magnitude of g_{HH} can be interpreted in the dispersion diagram as the displacement of the LP away from the expected crossing between the SLR and the HH ($K_{||}$ = ±2.3 μm⁻¹) (**Figure 4a**). Through two cycles of V_{app} and V_{dis} , the coupling strength decreases and recovers. Using our electrochemical cell, we observed that during the second cycle of V_{app} , g_{HH} contracted by 33% since an estimated 39.5% of NPLs had their excitonic transitions occluded and hence effectively segregated from the cavity (**Figure 4b**). The obvious band bending of the LP (teal) was reduced, and the LP can no longer be as clearly distinguished from the HH or SLR modes (white), and hence only weak coupling is present.^{2,53} Through the third and fourth cycles, the band-bending continues to reduce, and the dispersion diagrams of the cavities with and without NPL become more similar. During the 5th cycle of V_{app} , 89% of emitters in the NPL film were bleached, and g_{HH} decreased significantly, resulting in a significant kink forming between the now nearly completely X-shaped dispersive SLR modes and the flat-banded CdSe film HH (**Figure 4c**).

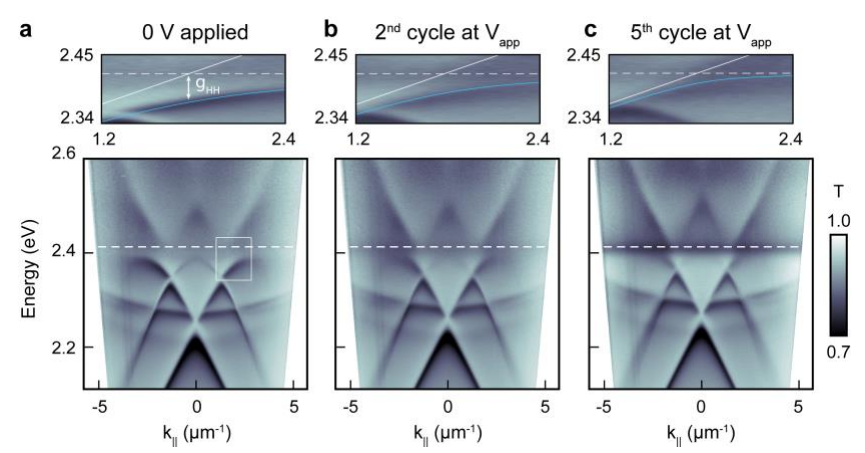


Figure 4: Repeated voltage and discharge cycles reduce and increase the coupling strength of the system. (a) Dispersion diagrams showing strong coupling before any voltage was applied. Inset is a detail view of the area of anti-crossing, with the heavy hole plotted in white, lower polariton fitting plotted in green, and the location of the original uncoupled SLR (calculated by coupling the Rayleigh anomaly from the empty lattice model with the LSP) in teal. (b) taken during the second cycle of $V_{app} = -1.78 \text{ V}$ vs. $Fc^{+/0}$ applied, and (c) the fifth cycle of V_{app} . Each potential was applied for 35 s and was followed by a discharge step of equal duration.

Because g_{HH} is directly proportional to N, g_{HH} would be expected to stabilize to the same value after each cycle. However, the continual decrease in coupling strength can be rationalized by estimating the number of electrons added and removed from the system. Calculations of the number of electrons in the NPL film during each potential step (Supporting Information) reveals that through the first cycle at V_{app} , 1.4×10^{16} electrons are added to the system (**Figure 5a**), resulting in a reduction in g_{HH} of 10 meV (from 45 to 35 meV) (**Figure 5b**). However, when the system is discharged in that cycle at -0.13 V vs. $Fc^{+/0}$ for 35 s, only 4.8×10^{15} electrons are removed from the film, and a recovery of 5 meV in g_{HH} was observed. After the first cycle, a net 9.2×10^{15} electrons are still in the film, corresponding to 66% of the initially added electrons,

and $g_{\rm HH}$ has only recovered 50% of the initial deficit by the end of the cycle (Supporting Information). This response is consistent through 5 cycles, after which accurately fitting the LP becomes challenging. The data suggests that strong coupling is not fully recovered at any point with a 35 s discharge step because the number of electrons added to the system are not fully removed within this timescale either.

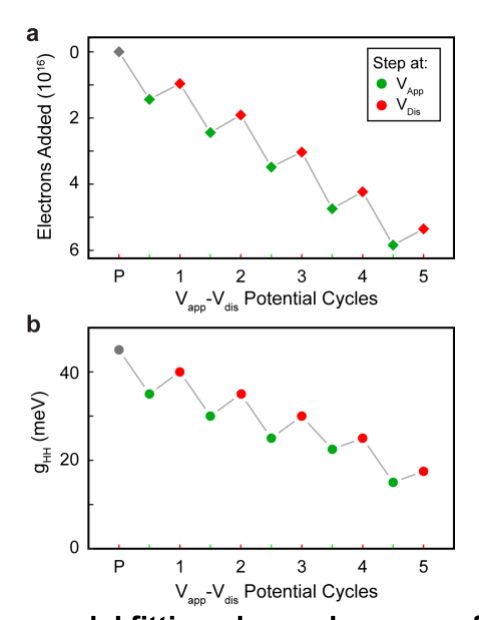


Figure 5. Jaynes-Cummings model fitting shows decrease of strong coupling as electrons are added into the system. (a) Plot of number of cumulative number of electrons added to the system ($x10^{16}$) after applying a voltage and after discharging for 35 s each. Grey points correspond to the system at the beginning of the experiment prior to applying any potential. Green corresponds to -1.78 V vs. Fc^{+/0} applied potential and red points correspond to discharging at -0.13 V. (b) Plot of g_{HH} values vs. applied potential or discharge step within each cycle.

The incomplete reduction of the film in the first cycle can be explained by the localization of electrochemically injected charge.⁵⁴⁻⁵⁶ As electrons are injected into the NPL film, cations from the electrolyte ([Bu₄N]⁺) are also drawn into the film voids.^{54, 56} The reduction of NPLs is restricted by the uptake of charge-compensating ions that depend on the size of the counter ion,

the void space of the NPL film, and the length of the NPL ligands.⁵⁴ Therefore, experimental differences in NPL film thickness or packing density can propagate to differences in NPL reduction efficiency. Injected charge can also be trapped in localized states at the NPL surface that will affect conduction band population and limit the full reduction of the NPL film in each cycle within experiment timescales.^{43, 47-48, 57-62} Charge trapping at NPL surface states may also result in chemically irreversible degradation.⁴⁷ The complications of electrochemically injected charge not only affect the addition of electrons, but also the efficient removal of all added electrons in the discharge step.^{43, 58} Additionally, injected charges can react with solvent impurities and prevent injected electrons from reducing the film.⁶³⁻⁶⁴ Ultimately, we attribute the incomplete removal of electrons and restoration of strong coupling during the cycling experiment to limitations on the rate or amount of charge that can be added or removed.^{56, 65}

In conclusion, we demonstrate that the coupling between CdSe NPLs and a plasmonic lattice cavity can be actively tuned across the strong and weak coupling regimes. The magnitude of the coupling lost and recovered correlated to the number of charges injected or removed from the NPL film. Tracking cumulative charge in an electrochemical system is useful for catalytic processes, helping to determine its efficiency in forming specific products. ⁶⁶ For improved recovery, cross-linking or ligand exchange procedures could be used to aid electron and electrolyte movement, and more robust emitters, such as core-shell NPLs, may withstand the harsh reductive environment better than oleate-capped NPLs. ⁶⁷ Our open cavity design and thin electrochemical cell show promise for active controlling strong coupling by applying electrochemical potentials. This work provides a foundation to understand the energetics of the upper and lower polariton, which is important for tuning the driving force of polariton-mediated redox reactions. Storing qubits in polaritons, tuning the driving force of photoelectrochemical reactions, and controlling polariton condensates will benefit from continued studies on external, *in-situ* control of coupling strength and polariton energetics.

ASSOCIATED CONTENT

Supporting Information

Lattice and NPL film substrate fabrication, experimental conditions of spectroelectrochemical experiments performed, sigmoidal fit equation parameters for quantification of nanoplatelet conduction band edge potential, FDTD modeling of uncoupled cavity, fitting procedures, spectroelectrochemical linear sweep voltammetry of coupled film and cavity, chronoamperometry of angle-dependent transmission spectroelectrochemical measurements, fitting with the coupled oscillator model and quantification of $g_{\rm HH}$ as a function of cycled potential (PDF)

Co-Corresponding Author

Jillian L. Dempsey-Department of Chemistry, University of North Carolina at Chapel Hill, Chapel Hill, North Carolina 27599-3290, United States; orcid.org/0000-0002-9459-4166; Email: dempseyi@email.unc.edu

Teri W. Odom – Department of Chemistry, Northwestern University, Evanston, Illinois 60208, United States; Department of Materials Science and Engineering, Northwestern University, Evanston, Illinois 60208, United States; https://orcid.org/0000-0002-8490-292X; Email: todom@northwestern.edu

Authors

Nathan G. Sinai – Department of Chemistry, Northwestern University, Evanston, Illinois 60208, United States; https://orcid.org/0000-0003-3507-992X; Email:

NathanSinai2027@u.northwestern.edu

Christian Y. Dones Lassalle-Department of Chemistry, University of North Carolina at Chapel Hill, Chapel Hill, North Carolina 27599-3290, United States; https://orcid.org/0009-0005-0317-457X; Email: chryad@email.unc.edu

Jennica E. Kelm-Department of Chemistry, University of North Carolina at Chapel Hill, Chapel Hill, North Carolina 27599-3290, United States; https://orcid.org/0000-0003-4310-7644; Email: iennica@email.unc.edu

Shreya K. Patel – Department of Chemistry, Northwestern University, Evanston, Illinois 60208, United States; https://orcid.org/0000-0003-0081-7937; Email: shreya.patel2@northwestern.edu Sang-Min Park – Department of Chemistry, Northwestern University, Evanston, Illinois 60208, United States; https://orcid.org/0000-0002-4306-0375; Email: Sang-minPark2025@u.northwestern.edu

Max J.H. Tan – Department of Chemistry, Northwestern University, Evanston, Illinois 60208, United States; https://orcid.org/0000-0002-6582-0670; Email: jintan2024@u.northwestern.edu

Author Contributions

The manuscript was written through contributions of all authors. All authors have given approval to the final version of the manuscript. *N.G.S, C.Y.D.L. and J.E.K contributed equally to this work.

Funding Sources

This work was supported by the National Science Foundation (NSF) Center for Chemical Innovation Center for Quantum Electrodynamics for Selective Transformations (QuEST) (NSF CHE-2124398).

Notes

The authors declare no competing financial interest.

Acknowledgements

The research was supported by the National Science Foundation (NSF) Center for Quantum Electrodynamics for Selective Transformations (QuEST) (Grant CHE-2124398). T.W.O. acknowledges support from the Vannevar Bush Faculty Fellowship from the U.S. Department of

Defense (DOD N00014-17-1-3023). This work made use of the NUFAB, EPIC, and SPID facilities of Northwestern University's NUANCE Center that has received support from the SHyNE Resource (NSF ECCS-2025633), the International Institute for Nanotechnology at Northwestern University (IIN), Northwestern's MRSEC Program (NSF DMR-1720139), and MRI (NSF DMR-1828676). S.K.P. acknowledges support from the National Science Foundation (NSF) MPS-Ascend Postdoctoral Research Fellowship (Grant No. 2316063). S.-M.P. and M.J.H.T. gratefully acknowledge support from the Ryan Fellowship and the International Institute for Nanotechnology at Northwestern University. This research was supported in part by the Quest high performance computing facility at Northwestern University, which is jointly supported by the Office of the Provost, the Office for Research, and Northwestern University Information Technology. We thank Francisco Freire Fernandez and Alex Sample at Northwestern University, Todd Krauss at Rochester University, Neil Spinner and Alex Peroff from Pine Research, and Alexandria Bredar from the University of North Carolina at Chapel Hill for their assistance with this project and insightful discussions.

References

- (1) Baranov, D. G.; Wersäll, M.; Cuadra, J.; Antosiewicz, T. J.; Shegai, T. Novel Nanostructures and Materials for Strong Light–Matter Interactions. *ACS Photonics* 2017, *5* (1), 24-42, DOI: 10.1021/acsphotonics.7b00674.
- (2) Dovzhenko, D. S.; Ryabchuk, S. V.; Rakovich, Y. P.; Nabiev, I. R. Light-matter interaction in the strong coupling regime: configurations, conditions, and applications. *Nanoscale* 2018, *10* (8), 3589-3605, DOI: 10.1039/c7nr06917k.
- (3) Ghosh, S.; Liew, T. C. H. Quantum computing with exciton-polariton condensates. *npj Quantum Information* 2020, 6 (1), DOI: 10.1038/s41534-020-0244-x.

- (4) Joseph, S.; Sarkar, S.; Joseph, J. Grating-Coupled Surface Plasmon-Polariton Sensing at a Flat Metal-Analyte Interface in a Hybrid-Configuration. *ACS Appl Mater Interfaces* 2020, *12* (41), 46519-46529, DOI: 10.1021/acsami.0c12525.
- (5) Freire-Fernández, F.; Sinai, N. G.; Tan, M. J. H.; Park, S.-M.; Koessler, E.; Krauss, T. D.; Huo, P.; Odom, T. W. Room-Temperature Polariton Lasing from CdSe core-only Nanoplatelets. arXiv:2404.08395 2024.
- (6) A. Thomas, L. L.-K., K. Nagarajan, R. M. A. Vergauwe, J. George, T. Chervy, A. Shalabney, E. Devaux, C. Genet, J. Moran, T. W. Ebbesen. Tilting a ground-state reactivity landscape by vibrational strong coupling. *Science* 2019, *363*, 615-619.
- (7) Mandal, A.; Krauss, T. D.; Huo, P. Polariton-Mediated Electron Transfer via Cavity Quantum Electrodynamics. *J Phys Chem B* 2020, *124* (29), 6321-6340, DOI: 10.1021/acs.jpcb.0c03227.
- (8) Martinez-Martinez, L. A.; Du, M.; R, F. R.; Kena-Cohen, S.; Yuen-Zhou, J. Polariton-Assisted Singlet Fission in Acene Aggregates. *J Phys Chem Lett* 2018, 9 (8), 1951-1957, DOI: 10.1021/acs.jpclett.8b00008.
- (9) Mandal, A.; Huo, P. Investigating New Reactivities Enabled by Polariton Photochemistry. *J Phys Chem Lett* 2019, *10* (18), 5519-5529, DOI: 10.1021/acs.jpclett.9b01599.
- (10) Zeng, H.; Perez-Sanchez, J. B.; Eckdahl, C. T.; Liu, P.; Chang, W. J.; Weiss, E. A.; Kalow, J. A.; Yuen-Zhou, J.; Stern, N. P. Control of Photoswitching Kinetics with Strong Light-Matter Coupling in a Cavity. *J Am Chem Soc* 2023, *145* (36), 19655-19661, DOI: 10.1021/jacs.3c04254.
- (11) Puro, R.; Van Schenck, J. D. B.; Center, R.; Holland, E. K.; Anthony, J. E.; Ostroverkhova, O. Exciton Polariton-Enhanced Photodimerization of Functionalized Tetracene. *The Journal of Physical Chemistry C* 2021, *125* (49), 27072-27083, DOI: 10.1021/acs.jpcc.1c06881.

- (12) Ramezani, M.; Berghuis, M.; Gómez Rivas, J. Strong light–matter coupling and exciton-polariton condensation in lattices of plasmonic nanoparticles [Invited]. *Journal of the Optical Society of America B* 2019, *36* (7), DOI: 10.1364/josab.36.000e88.
- (13) Moilanen, A. J.; Hakala, T. K.; Törmä, P. Active Control of Surface Plasmon–Emitter Strong Coupling. *ACS Photonics* 2017, *5* (1), 54-64, DOI: 10.1021/acsphotonics.7b00655.
- (14) Liu, W.; Wang, Y.; Zheng, B.; Hwang, M.; Ji, Z.; Liu, G.; Li, Z.; Sorger, V. J.; Pan, A.; Agarwal, R. Observation and Active Control of a Collective Polariton Mode and Polaritonic Band Gap in Few-Layer WS(2) Strongly Coupled with Plasmonic Lattices. *Nano Lett* 2020, *20* (1), 790-798, DOI: 10.1021/acs.nanolett.9b05056.
- (15) Yang, A.; Hoang, T. B.; Dridi, M.; Deeb, C.; Mikkelsen, M. H.; Schatz, G. C.; Odom, T. W. Real-time tunable lasing from plasmonic nanocavity arrays. *Nat Commun* 2015, *6*, 6939, DOI: 10.1038/ncomms7939.
- (16) Wen, J.; Wang, H.; Wang, W.; Deng, Z.; Zhuang, C.; Zhang, Y.; Liu, F.; She, J.; Chen, J.; Chen, H.; Deng, S.; Xu, N. Room-Temperature Strong Light-Matter Interaction with Active Control in Single Plasmonic Nanorod Coupled with Two-Dimensional Atomic Crystals. *Nano Lett* 2017, *17* (8), 4689-4697, DOI: 10.1021/acs.nanolett.7b01344.
- (17) Xiong, W. Molecular Vibrational Polariton Dynamics: What Can Polaritons Do? *Acc Chem Res* 2023, *56* (7), 776-786, DOI: 10.1021/acs.accounts.2c00796.
- (18) Kagilev, A. A.; Gafurov, Z. N.; Kantyukov, A. O.; Mikhailov, I. K.; Yakhvarov, D. G. The power of in situ spectroelectrochemistry for redox study of organometallic and coordination compounds. *Journal of Solid State Electrochemistry* 2023, *28* (3-4), 897-910, DOI: 10.1007/s10008-023-05765-7.
- (19) Lee, B.; Liu, W.; Naylor, C. H.; Park, J.; Malek, S. C.; Berger, J. S.; Johnson, A. T. C.; Agarwal, R. Electrical Tuning of Exciton-Plasmon Polariton Coupling in Monolayer MoS(2) Integrated with Plasmonic Nanoantenna Lattice. *Nano Lett* 2017, *17* (7), 4541-4547, DOI: 10.1021/acs.nanolett.7b02245.

- (20) Graf, A.; Held, M.; Zakharko, Y.; Tropf, L.; Gather, M. C.; Zaumseil, J. Electrical pumping and tuning of exciton-polaritons in carbon nanotube microcavities. *Nat Mater* 2017, *16* (9), 911-917, DOI: 10.1038/nmat4940.
- (21) Pietron, J. J.; Fears, K. P.; Owrutsky, J. C.; Simpkins, B. S. Electrochemical Modulation of Strong Vibration–Cavity Coupling. *ACS Photonics* 2019, 7 (1), 165-173, DOI: 10.1021/acsphotonics.9b01339.
- (22) Ahn, W.; Simpkins, B. S. Spectroelectrochemical measurement and modulation of exciton-polaritons. *APL Photonics* 2020, *5* (7), DOI: 10.1063/5.0012528.
- (23) Yang, Y.; Chikkaraddy, R.; Lin, Q.; Clarke, D. D. A.; Wigger, D.; Baumberg, J. J.; Hess, O. Electrochemically Switchable Multimode Strong Coupling in Plasmonic Nanocavities. *Nano Lett* 2024, *24* (1), 238-244, DOI: 10.1021/acs.nanolett.3c03814.
- (24) Gong, K.; Zeng, Y.; Kelley, D. F. Extinction Coefficients, Oscillator Strengths, and Radiative Lifetimes of CdSe, CdTe, and CdTe/CdSe Nanocrystals. *The Journal of Physical Chemistry C* 2013, *117* (39), 20268-20279, DOI: 10.1021/jp4065449.
- (25) Geiregat, P.; Roda, C.; Tanghe, I.; Singh, S.; Di Giacomo, A.; Lebrun, D.; Grimaldi, G.; Maes, J.; Van Thourhout, D.; Moreels, I.; Houtepen, A. J.; Hens, Z. Localization-limited exciton oscillator strength in colloidal CdSe nanoplatelets revealed by the optically induced stark effect. *Light Sci Appl* 2021, *10* (1), 112, DOI: 10.1038/s41377-021-00548-z.
- (26) Leistikow, M. D.; Johansen, J.; Kettelarij, A. J.; Lodahl, P.; Vos, W. L. Size-dependent oscillator strength and quantum efficiency of CdSe quantum dots controlled via the local density of states. *Physical Review B* 2009, *79* (4), DOI: 10.1103/PhysRevB.79.045301.
- (27) Querner, C.; Reiss, P.; Sadki, S.; Zagorska, M.; Pron, A. Size and ligand effects on the electrochemical and spectroelectrochemical responses of CdSe nanocrystals. *Phys Chem Chem Phys* 2005, 7 (17), 3204-9, DOI: 10.1039/b508268b.

- (28) Sun, H.; Buhro, W. E. Reversible Z-Type to L-Type Ligand Exchange on Zinc-Blende Cadmium Selenide Nanoplatelets. *Chemistry of Materials* 2020, *32* (13), 5814-5826, DOI: 10.1021/acs.chemmater.0c01712.
- (29) Bertolazzi, S.; Gobbi, M.; Zhao, Y.; Backes, C.; Samori, P. Molecular chemistry approaches for tuning the properties of two-dimensional transition metal dichalcogenides. *Chem Soc Rev* 2018, *47* (17), 6845-6888, DOI: 10.1039/c8cs00169c.
- (30) Chen, X.; McDonald, A. R. Functionalization of Two-Dimensional Transition-Metal Dichalcogenides. *Adv Mater* 2016, *28* (27), 5738-46, DOI: 10.1002/adma.201505345.
- (31) Winkler, J. M.; Rabouw, F. T.; Rossinelli, A. A.; Jayanti, S. V.; McPeak, K. M.; Kim, D. K.; le Feber, B.; Prins, F.; Norris, D. J. Room-Temperature Strong Coupling of CdSe Nanoplatelets and Plasmonic Hole Arrays. *Nano Lett* 2019, *19* (1), 108-115, DOI: 10.1021/acs.nanolett.8b03422.
- (32) Qiu, L.; Mandal, A.; Morshed, O.; Meidenbauer, M. T.; Girten, W.; Huo, P.; Vamivakas, A. N.; Krauss, T. D. Molecular Polaritons Generated from Strong Coupling between CdSe Nanoplatelets and a Dielectric Optical Cavity. *J Phys Chem Lett* 2021, *12* (20), 5030-5038, DOI: 10.1021/acs.jpclett.1c01104.
- (33) Yeltik, A.; Delikanli, S.; Olutas, M.; Kelestemur, Y.; Guzelturk, B.; Demir, H. V. Experimental Determination of the Absorption Cross-Section and Molar Extinction Coefficient of Colloidal CdSe Nanoplatelets. *The Journal of Physical Chemistry C* 2015, *119* (47), 26768-26775, DOI: 10.1021/acs.jpcc.5b09275.
- (34) Sample, A. D.; Guan, J.; Hu, J.; Reese, T.; Cherqui, C. R.; Park, J. E.; Freire-Fernandez, F.; Schaller, R. D.; Schatz, G. C.; Odom, T. W. Strong Coupling Between Plasmons and Molecular Excitons in Metal-Organic Frameworks. *Nano Lett* 2021, *21* (18), 7775-7780, DOI: 10.1021/acs.nanolett.1c02740.
- (35) Sample, A. D.; Guan, J.; Hu, J.; Freire-Fernández, F.; Park, S.-M.; Schaller, R. D.; Schatz, G. C.; Odom, T. W. Polariton Formation from Soret Band Excitons in Metal–Organic

- Frameworks and Plasmonic Lattices. *The Journal of Physical Chemistry C* 2022, *126* (44), 18778-18783, DOI: 10.1021/acs.jpcc.2c05464.
- (36) Deng, S.; Park, J. E.; Kang, G.; Guan, J.; Li, R.; Schatz, G. C.; Odom, T. W. Interfacial engineering of plasmonic nanoparticle metasurfaces. *Proc Natl Acad Sci U S A* 2022, *119* (22), e2202621119, DOI: 10.1073/pnas.2202621119.
- (37) Deng, S.; Zhang, B.; Choo, P.; Smeets, P. J. M.; Odom, T. W. Plasmonic Photoelectrocatalysis in Copper-Platinum Core-Shell Nanoparticle Lattices. *Nano Lett* 2021, *21* (3), 1523-1529, DOI: 10.1021/acs.nanolett.0c05029.
- (38) Kravets, V. G.; Kabashin, A. V.; Barnes, W. L.; Grigorenko, A. N. Plasmonic Surface Lattice Resonances: A Review of Properties and Applications. *Chem Rev* 2018, *118* (12), 5912-5951, DOI: 10.1021/acs.chemrev.8b00243.
- (39) Wang, D.; Guan, J.; Hu, J.; Bourgeois, M. R.; Odom, T. W. Manipulating Light-Matter Interactions in Plasmonic Nanoparticle Lattices. *Acc Chem Res* 2019, *52* (11), 2997-3007, DOI: 10.1021/acs.accounts.9b00345.
- (40) Tan, M. J. H.; Park, J. E.; Freire-Fernandez, F.; Guan, J.; Juarez, X. G.; Odom, T. W. Lasing Action from Quasi-Propagating Modes. *Adv Mater* 2022, *34* (34), e2203999, DOI: 10.1002/adma.202203999.
- (41) Elgrishi, N.; Rountree, K. J.; McCarthy, B. D.; Rountree, E. S.; Eisenhart, T. T.; Dempsey, J. L. A Practical Beginner's Guide to Cyclic Voltammetry. *Journal of Chemical Education* 2017, 95 (2), 197-206, DOI: 10.1021/acs.jchemed.7b00361.
- (42) Schimpf, A. M.; Knowles, K. E.; Carroll, G. M.; Gamelin, D. R. Electronic doping and redox-potential tuning in colloidal semiconductor nanocrystals. *Acc Chem Res* 2015, *48* (7), 1929-37, DOI: 10.1021/acs.accounts.5b00181.
- (43) Rinehart, J. D.; Schimpf, A. M.; Weaver, A. L.; Cohn, A. W.; Gamelin, D. R.
 Photochemical electronic doping of colloidal CdSe nanocrystals. *J Am Chem Soc* 2013, 135
 (50), 18782-5, DOI: 10.1021/ja410825c.

- (44) Shim, M.; Guyot-Sionnest, P. n-type colloidal semiconductor nanocrystals. *Nature* 2000, 407 (6807), 981-983, DOI: 10.1038/35039577.
- (45) Ashokan, A.; Han, J.; Hutchison, J. A.; Mulvaney, P. Spectroelectrochemistry of CdSe/Cd(x)Zn(1-x)S Nanoplatelets. *ACS Nano* 2023, DOI: 10.1021/acsnano.2c09298.
- (46) Spittel, D.; Poppe, J.; Meerbach, C.; Ziegler, C.; Hickey, S. G.; Eychmuller, A. Absolute Energy Level Positions in CdSe Nanostructures from Potential-Modulated Absorption Spectroscopy (EMAS). *ACS Nano* 2017, *11* (12), 12174-12184, DOI: 10.1021/acsnano.7b05300.
- (47) Hartley, C. L.; Dempsey, J. L. Electron-Promoted X-Type Ligand Displacement at CdSe Quantum Dot Surfaces. *Nano Lett* 2019, *19* (2), 1151-1157, DOI: 10.1021/acs.nanolett.8b04544.
- (48) Hartley, C. L.; Dempsey, J. L. Revealing the Molecular Identity of Defect Sites on PbS Quantum Dot Surfaces with Redox-Active Chemical Probes. *Chemistry of Materials* 2021, 33 (7), 2655-2665, DOI: 10.1021/acs.chemmater.1c00520.
- (49) Guan, J.; Sagar, L. K.; Li, R.; Wang, D.; Bappi, G.; Wang, W.; Watkins, N.; Bourgeois, M. R.; Levina, L.; Fan, F.; Hoogland, S.; Voznyy, O.; de Pina, J. M.; Schaller, R. D.; Schatz, G. C.; Sargent, E. H.; Odom, T. W. Quantum Dot-Plasmon Lasing with Controlled Polarization Patterns. *ACS Nano* 2020, *14* (3), 3426-3433, DOI: 10.1021/acsnano.9b09466.
- (50) Guan, J.; Sagar, L. K.; Li, R.; Wang, D.; Bappi, G.; Watkins, N. E.; Bourgeois, M. R.; Levina, L.; Fan, F.; Hoogland, S.; Voznyy, O.; Martins de Pina, J.; Schaller, R. D.; Schatz, G. C.; Sargent, E. H.; Odom, T. W. Engineering Directionality in Quantum Dot Shell Lasing Using Plasmonic Lattices. *Nano Lett* 2020, *20* (2), 1468-1474, DOI: 10.1021/acs.nanolett.9b05342.
- (51) Li, L.; Ouyang, Y.; Ma, L.; Sun, H.; Chen, Y.; Wu, M.; Qi, Z.; Wu, W. Reflection-type surface lattice resonances in all-metal metasurfaces for refractive index sensing. *Photonics Research* 2023, *11* (12), DOI: 10.1364/prj.502199.

- (52) Pourjamal, S.; Kataja, M.; Maccaferri, N.; Vavassori, P.; van Dijken, S. Hybrid Ni/SiO2/Au dimer arrays for high-resolution refractive index sensing. *Nanophotonics* 2018, *7* (5), 905-912, DOI: 10.1515/nanoph-2018-0013.
- (53) Cao, E.; Lin, W.; Sun, M.; Liang, W.; Song, Y. Exciton-plasmon coupling interactions: from principle to applications. *Nanophotonics* 2018, *7* (1), 145-167, DOI: 10.1515/nanoph-2017-0059.
- (54) Boehme, S. C.; Wang, H.; Siebbeles, L. D. A.; Vanmaekelbergh, D.; Houtepen, A. J. Electrochemical Charging of CdSe Quantum Dot Films: Dependence on Void Size and Counterion Proximity. *ACS Nano* 2013, 7 (3), 2500-2508, DOI: 10.1021/nn3058455.
- (55) Gudjonsdottir, S.; van der Stam, W.; Kirkwood, N.; Evers, W. H.; Houtepen, A. J. The Role of Dopant Ions on Charge Injection and Transport in Electrochemically Doped Quantum Dot Films. *J Am Chem Soc* 2018, *140* (21), 6582-6590, DOI: 10.1021/jacs.8b01347.
- (56) Eren, H.; Bednarz, R. J.; Alimoradi Jazi, M.; Donk, L.; Gudjonsdottir, S.; Bohlander, P.; Eelkema, R.; Houtepen, A. J. Permanent Electrochemical Doping of Quantum Dot Films through Photopolymerization of Electrolyte Ions. *Chem Mater* 2022, *34* (9), 4019-4028, DOI: 10.1021/acs.chemmater.2c00199.
- (57) Tsui, E. Y.; Hartstein, K. H.; Gamelin, D. R. Selenium Redox Reactivity on Colloidal CdSe Quantum Dot Surfaces. *J Am Chem Soc* 2016, *138* (35), 11105-8, DOI: 10.1021/jacs.6b06548.
- (58) Tsui, E. Y.; Carroll, G. M.; Miller, B.; Marchioro, A.; Gamelin, D. R. Extremely Slow Spontaneous Electron Trapping in Photodoped n-Type CdSe Nanocrystals. *Chem Mater* 2017, 29 (8), 3754-3762, DOI: 10.1021/acs.chemmater.7b00839.
- (59) Rinehart, J. D.; Weaver, A. L.; Gamelin, D. R. Redox brightening of colloidal semiconductor nanocrystals using molecular reductants. *J Am Chem Soc* 2012, *134* (39), 16175-7, DOI: 10.1021/ja307996b.
- (60) du Fosse, I.; Boehme, S. C.; Infante, I.; Houtepen, A. J. Dynamic Formation of Metal-Based Traps in Photoexcited Colloidal Quantum Dots and Their Relevance for

- Photoluminescence. *Chem Mater* 2021, *33* (9), 3349-3358, DOI: 10.1021/acs.chemmater.1c00561.
- (61) van der Stam, W.; du Fosse, I.; Grimaldi, G.; Monchen, J. O. V.; Kirkwood, N.; Houtepen, A. J. Spectroelectrochemical Signatures of Surface Trap Passivation on CdTe Nanocrystals.
 Chem Mater 2018, 30 (21), 8052-8061, DOI: 10.1021/acs.chemmater.8b03893.
- (62) Schimpf, A. M.; Gunthardt, C. E.; Rinehart, J. D.; Mayer, J. M.; Gamelin, D. R. Controlling carrier densities in photochemically reduced colloidal ZnO nanocrystals: size dependence and role of the hole quencher. *J Am Chem Soc* 2013, *135* (44), 16569-77, DOI: 10.1021/ja408030u.
- (63) Lakhwani, G.; Roijmans, R. F. H.; Kronemeijer, A. J.; Gilot, J.; Janssen, R. A. J.; Meskers, S. C. J. Probing Charge Carrier Density in a Layer of Photodoped ZnO Nanoparticles by Spectroscopic Ellipsometry. *The Journal of Physical Chemistry C* 2010, *114* (35), 14804-14810, DOI: 10.1021/jp104846h.
- (64) Gooding, A. K.; Gómez, D. E.; Mulvaney, P. The Effects of Electron and Hole Injection on the Photoluminescence of CdSe/CdS/ZnS Nanocrystal Monolayers. *ACS Nano* 2008, *2* (4), 669-676, DOI: 10.1021/nn7003469.
- (65) Guyot-Sionnest, P.; Wang, C. Fast Voltammetric and Electrochromic Response of Semiconductor Nanocrystal Thin Films. *The Journal of Physical Chemistry B* 2003, *107* (30), 7355-7359, DOI: 10.1021/jp0275084.
- (66) Dutta, N.; Bagchi, D.; Chawla, G.; Peter, S. C. A Guideline to Determine Faradaic Efficiency in Electrochemical CO2 Reduction. *ACS Energy Letters* 2024, 9 (1), 323-328, DOI: 10.1021/acsenergylett.3c02362.
- (67) Lorenzon, M.; Christodoulou, S.; Vaccaro, G.; Pedrini, J.; Meinardi, F.; Moreels, I.; Brovelli, S. Reversed oxygen sensing using colloidal quantum wells towards highly emissive photoresponsive varnishes. *Nat Commun* 2015, *6*, 6434, DOI: 10.1038/ncomms7434.